ELSEVIER

Journal of Atmospheric and Solar-Terrestrial Physics 66 (2004) 323–331

Journal of ATMOSPHERIC AND SOLAR-TERRESTRIAL PHYSICS

www.elsevier.com/locate/jastp

Solar cycle control of the magnetic cloud polarity and the geoeffectiveness

Yan Li*, Janet Luhmann

Space Sciences Laboratory, University of California, 7 Gauss Way, Berkeley, CA 94720-7450, USA

Received 3 September 2003; received in revised form 12 November 2003; accepted 11 December 2003

Abstract

Magnetic clouds are surveyed in interplanetary magnetic field (IMF) and solar wind data from ACE, WIND, ISEE3, and IMP8 spacecraft. The annual frequency distribution of the bipolar magnetic clouds combined with PVO results by Mulligan et al. (Geophys. Res. Lett. 25 (1998) 2959) shows that the occurrence of SN magnetic clouds prevails over NS magnetic clouds in an odd solar cycle, and the reverse is true for an even solar cycle. The prevailing polarity cases decrease in number towards the solar minimum, while the secondary polarity clouds start to increase in number, only becoming predominant after the later part of the declining phase. Therefore, the predominance of the magnetic cloud polarity reverses within the later part of the declining phase near the solar minimum, but does not coincide with either the solar minimum when the new polarity sunspots begin to emerge or the solar maximum when the large scale solar polar field reverses. The annual frequency distribution of the total number of bipolar magnetic clouds and total number of unipolar magnetic clouds is not well ordered by the solar cycle. Perhaps both solar polar field cycle and the Hale active region polarity cycle may affect the magnetic cloud polarity. Magnetic clouds from all four spacecraft during 1978–2002 are evaluated for their geoeffectiveness. Overall statistics show that NS and SN magnetic clouds are equally geoeffective. We also found that both the cloud portion and sheath portion during the magnetic cloud period are important in causing geomagnetic storms. The magnetic cloud disturbance periods are the primary cause of one-third of the total number of geomagnetic storms analyzed, but are responsible for the most intense storms.

Keywords: Space weather; Coronal mass ejections; Magnetic clouds; Geomagnetic storms

1. Introduction

Despite great interest in and much effort devoted to coronal mass ejection (CME) genesis and interplanetary CME (ICME) origins, many questions remain. In particular, the connection between ICME, CME and the source region near the solar surface is not well understood. A number of authors have studied the magnetic structure of the magnetic clouds, a subset of ICMEs (Gosling, 1990) and its solar cycle evolution by means of interplanetary magnetic field (IMF) and solar wind in situ observations. Magnetic clouds are observed as smoothly rotating magnetic field vector through a large angle, low magnetic variance and enhanced field magnitude intervals of many hours duration in interplanetary magnetic field observations (e.g., Burlaga, 1991). These periods are distinguished from the ambient solar wind. The simplest interpretation of the magnetic cloud structure is a cylindrical magnetic fluxrope (Mulligan and Russell, 2001) that is either expelled from the Sun or formed during the process of the coronal mass ejection. The internal field and plasma parameters of the fluxrope are observed when a spacecraft flies through the structure. The magnetic structure and temporal evolution of the magnetic clouds provide especially useful information for understanding the ICMEs, and their related CME origins because they are well defined and are

* Corresponding author. Fax: +1-510-643-8302.
E-mail address: yanli@ssl.berkeley.edu (Y. Li).

1364-6826/$ - see front matter © 2004 Elsevier Ltd. All rights reserved.
doi:10.1016/j.jastp.2003.12.001

good candidates for comparison with CME models. Of special importance is the bipolar signature of the out of ecliptic plane (B_z) component, both due to its implication for the solar source and its role in the ICME geoeffects. Zhang and Burlaga (1988) using IMP8/ISEE3 data and Bothmer and Schwenn (1998) using Helios data found that the majority of the magnetic clouds have south leading field and north trailing field (SN magnetic clouds hereafter) during the period 1974–1982. Bothmer and Rust (1997) found 19 SN magnetic clouds and 5 NS (north leading field and south trailing field) magnetic clouds during 1974–1981; but 14 NS magnetic clouds and 3 SN magnetic clouds during 1982 and 1991 using the OMNI data set, and presented their statistical results as pie charts. They interpreted the reversal of the magnetic cloud polarities as related to Hα filaments and the field arcades over the filaments, the magnetic field orientation of which reverses with the solar cycle. Using Pioneer Venus Obiter (PVO) data spanning 1979 to 1988, from the maximum of cycle 21 to near maximum of cycle 22, Mulligan et al. (1998) found a solar cycle dependence of the bipolar B_z signature that they presented as a histogram of annual occurrence frequency as a function of time. They also pointed out that bipolar magnetic clouds occur near solar minimum to maximum when the large-scale neutral line and coronal streamer belt is more flat and equatorial; while the peak of occurrence of unipolar (possibly highly inclined fluxropes) magnetic clouds is in the declining phase when the neutral line and streamer belt are highly inclined with respect to the ecliptic plane. These authors concluded that the magnetic clouds are controlled by the streamer belt-related coronal large-scale magnetic field.

Zhang and Burlaga (1988) found in their data set that SN magnetic clouds caused larger geomagnetic storms than the NS magnetic clouds, but attributed that to the fact that the particular group of SN magnetic clouds they studied is associated with larger solar wind speeds during the ICMEs. On the other hand, Fenrich and Luhmann (1998) argued that NS magnetic clouds might cause larger geomagnetic storms versus SN magnetic clouds under the circumstances that the magnetic clouds should be followed and compressed from behind by fast solar wind streams, which they found occurred in 40–45% of magnetic clouds, independent of polarity. No statistical results were shown in terms of which of the two types of magnetic clouds in fact caused larger geomagnetic storms in their 29 events.

In this paper, we further study the polarity behavior of the B_z component of the magnetic clouds, its temporal evolution and consequences using extended data sets. Considering data quality and coverage, the solar wind and IMF data that are suitable to this study are primarily from observations on board WIND and ACE during 1995 and 2002, and ISEE3 during 1978 and 1982. We compare with the results from PVO data by Mulligan et al. (1998). IMP8 data are included in some of the statistical studies. The geoeffectiveness of the identified magnetic clouds is also examined for any dependence on magnetic cloud polarities and other aspects.

2. Observations and event selections

Our analysis relies on the continuity of solar wind plasma and IMF measurements for obtaining magnetic cloud annual statistics and solar cycle evolution. The study also requires consistent identification and characterization of the magnetic clouds. We have surveyed in situ observations of the IMF and solar wind parameters measured by instruments on board ISEE3, WIND, ACE and IMP8 spacecrafts (von Rosenvinge, 1982; Russell, 1995 and references therein; Garrard et al., 1998; Paularena and King, 1999). In particular, we use the magnetometer data in GSM coordinates, proton temperature, density, and solar wind bulk velocity. We also use Kyoto Dst index for geomagnetic storms. ACE data (from 02/1998 to 12/2002) have the best quality and the spacecraft is situated at the Sun–Earth Lagrange-1 (or L1) point, providing $\sim$100% coverage in time of the upstream solar wind. We use ACE 1-min data that are made available at the UCLA solar wind data server website (http://www-ssc.igpp.ucla.edu/forms/polar/corr_data.html) from year 2002 back to the beginning of the mission in February 1998. From January 1998 back to January 1995, we use WIND 1 min data that are also available at the UCLA solar wind data server website, the quality of which is also excellent. During the time period used, the WIND spacecraft had an Earth orbit, but only entered the magnetosphere a fraction of the time $\sim$2.7%. During the missing period of the solar wind observations, only one geomagnetic storm occurred. Therefore we consider that WIND data coverage is adequate for this study, i.e., the number of missing events will not impact our conclusion in any significant way. We obtained 5 min ISEE3 data from the same UCLA source. The ISEE3 spacecraft was situated at the L1 point, providing upstream magnetometer data from 08/1978 to 12/1982. The solar wind proton data were only available from 08/78 to 02/80. Electron temperature, density, and bulk velocity data are used for the period 02/80 to 10/82. In the last 2 months of 1982, there were no plasma data at all. Magnetic field data were used alone, which adds some difficulty and uncertainty in identifying magnetic clouds or cloud boundaries in the 2 months. For time period 01/78 to 08/78, we use IMP8 data to make up the full year coverage, because this study requires annual occurrence of magnetic clouds. IMP8 data from 1978 to 1992 with 5 min time resolution from the UCLA source are included in this study. The IMP8 data have good quality, but the spacecraft was in the magnetosheath or magnetosphere instead of in the solar wind for 47% of the time, which together with data gaps resulted in less than 50% coverage. Thus the total number of magnetic clouds in the year 1978 may be underestimated.

Magnetic clouds in the solar wind are identified using the following criteria established by Burlaga (1991), which are consistent with the study of Mulligan et al. (1998). The magnetic field vector rotates through a large angle on the time scale of the order of a day; the magnitude of the field is enhanced during the interval concerned; the magnetic variance

and the proton temperature are relatively low. The inclusion of plasma data in the identification is important because there are often ambiguities, e.g. between magnetic fields in the ICME sheath and in the ejecta. We use the same convention and definition in Mulligan et al. (1998) for NS and SN bipolar magnetic clouds and N or S unipolar (or highly inclined) magnetic clouds.

3. Magnetic cloud B_z polarity and the solar cycle evolution

3.1. Results from the data

An example of a typical magnetic cloud in May 15, 1997 is presented in Fig. 1. Shown from top to bottom are proton temperature, density, and solar wind bulk velocity, solar wind dynamic pressure, IMF B_x, B_y, B_z (in GSM) and magnetic field magnitude B_t, and finally Kyoto D_{st} geomagnetic storm index from the web server at http://swdcdb.kugi.kyoto-u.ac.jp/dstdir/. The boundaries of the ICME sheath (with enhanced magnetic field strength and oscillating field direction, and increased proton temperature, density and speed) and the cloud are marked with vertical dotted lines. This is a southward B_z leading and northward following magnetic cloud, or SN magnetic cloud. A negative excursion of the D_{st} value marks a geomagnetic storm. A storm with the minimum D_{st} of −115 nT is caused by the disturbed period of this magnetic cloud.

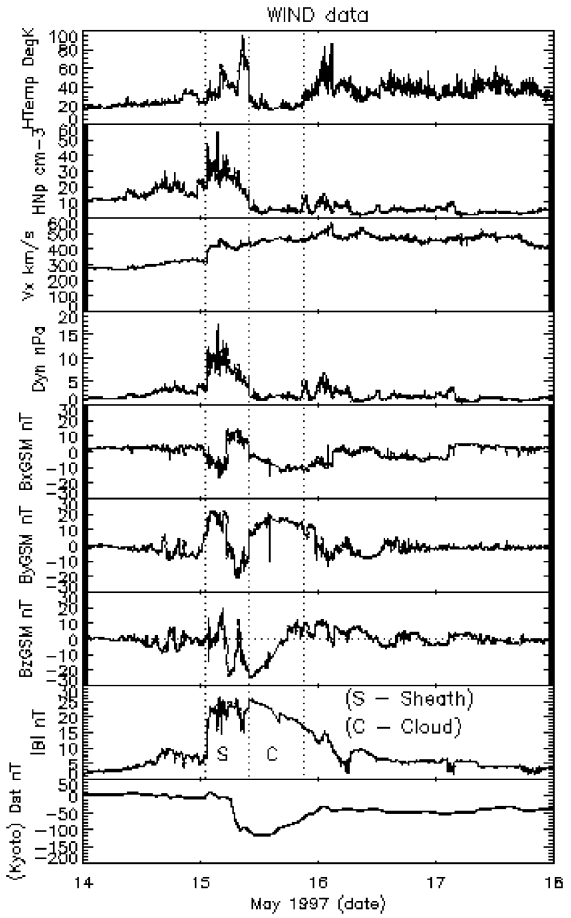

Fig. 1. A magnetic cloud in May 15, 1997. From top to bottom are proton temperature, density, and solar wind bulk velocity, solar wind dynamic pressure, IMF B_x, B_y, B_z (in GSM) and magnetic field magnitude B_t, and finally Kyoto D_{st} index. The boundaries of the ICME sheath and the cloud are marked with vertical dotted lines. A geomagnetic storm of minimum D_{st} value—115 nT is seen in the bottom panel.

A total of 9 NS magnetic clouds and 22 SN magnetic clouds are identified from the 5-year period of ISEE3/IMP8 data during 1978–1982. From 3 years of WIND data and 5 years of ACE data during 1995–2002, a total of 10 NS magnetic clouds and 36 SN magnetic clouds are identified. The annual frequency distribution of the bipolar magnetic clouds is shown (black bars) in Fig. 2 as a function of time with the solar polar magnetic fields of the corresponding cycles shown above and the sunspot numbers of the same cycles below. Both periods were in an odd cycle. The ISEE3 period was from a year before the maximum and three years into the declining phase of cycle 21 and the WIND-ACE period was from the minimum through the rising phase to 2 years after the maximum of cycle 23. Both periods have SN magnetic clouds predominant. The tendency for a solar cycle dependence can be seen in both periods, details of which will be discussed in later sections. There are also 6 NS magnetic clouds and 2 SN magnetic clouds identified during 1983–1992 covering most of cycle 22 using IMP8 data, but these are not suitable to be included in Fig. 2 for this study due to the insufficient upstream time coverage of IMP8. A part of the annual occurrence statistics from PVO (Pioneer Venus Obiter) data obtained by Mulligan et al. (1998) is included in Fig. 2 as gray bars. While the PVO magnetic clouds are not selected by the same authors and the normalization is slightly different due to the sampling coverage in the PVO orbit, they give an indication of the continuous trend in solar cycle behavior.

Also identified are 3 N and 4 S unipolar magnetic clouds during 1978–1982, and 5 N and 13 S unipolar magnetic clouds during 1995–2002. Fig. 3 presents the annual frequency distribution of the bipolar (both NS and SN) magnetic clouds and unipolar magnetic clouds. The total number of bipolar MCs shows little trend with the solar cycle. The total number of unipolar MC distribution similarly shows no clear solar cycle trend.

3.2. Discussions on magnetic cloud polarity statistics

The above results show that the polarity of the magnetic clouds have SN field rotation for majority of the events over NS field rotation in both periods from 1978 to 1982 in solar cycle 21 and from 1995 to 2002 in solar cycle 23.

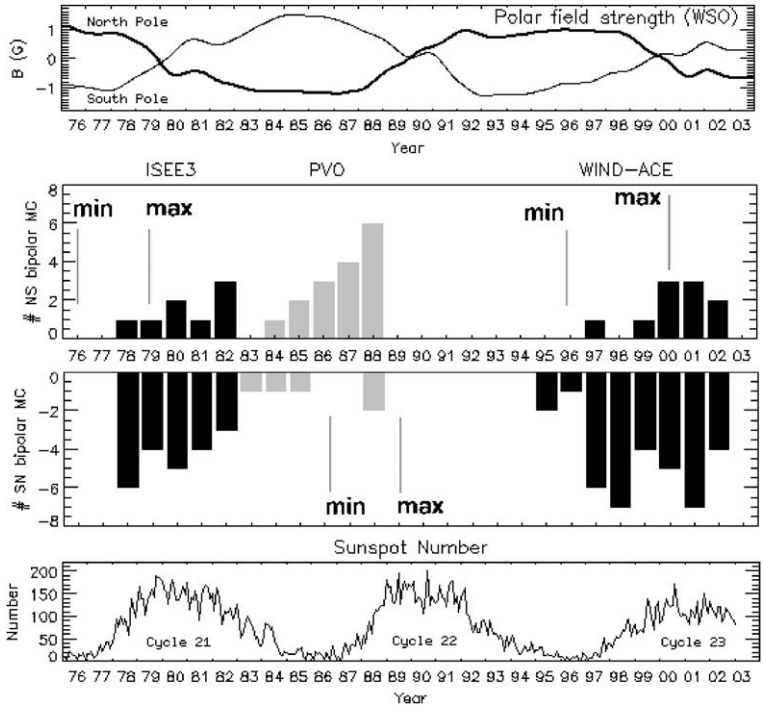

Fig. 2. Upper panel: solar polar field strength of cycle 21–23. Middle panel: annual frequency distribution of bipolar magnetic clouds from ISEE3 data (78–82) during the solar maximum and part of the declining phase of cycle 21 (black bars), part of Mulligan et al.'s (1998) PVO results (gray bars) in the rising phase of cycle 22 and from WIND data (95–97) and ACE data (98–02) during the solar minimum, the rising phase, the maximum and two years into the declining phase of cycle 23. Lower panel: the monthly sunspot numbers of solar cycle 21–23.

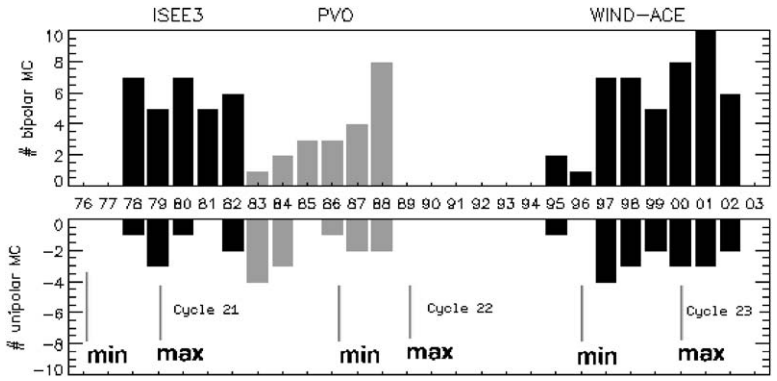

Fig. 3. Top: Annual frequency distribution of magnetic clouds with bipolar B_z as a function of time. Bottom: Same but for unipolar magnetic clouds. Magnetic clouds in ISEE3 and WIND-ACE periods are shown in black bars and gray bars in PVO period.

These findings agree with previous studies (Zhang and Burlaga, 1988; Bothmer and Rust, 1997; Bothmer and Schwenn, 1998). Further we explored the solar cycle evolution of the magnetic cloud polarity by annual occurrence frequency as a function of time. The ISEE3 data cover mostly the declining phase of cycle 21, while the WIND-ACE data cover the entire rising phase of cycle 23. The SN magnetic clouds in cycle 21 show a tendency of decreasing in number as the declining phase proceeds. Combined with the earlier PVO results of Mulligan et al. (1998), the magnetic cloud polarity appears to reverse so that the NS magnetic clouds prevail during the later half of the declining phase, and the NS magnetic clouds continue to increase in occurrence towards the next solar maximum.

The SN magnetic clouds in cycle 23 have an abrupt increase in number right after the solar minimum, then throughout the rising phase of cycle 23 the number of occurrences of SN magnetic clouds simply oscillates, no clear trend, which differs from the PVO results that had a monotonic increase over the rising phase of cycle 22. However, the exact fashion of the trend perhaps cannot be interpreted with great significance, considering the randomness of CMEs and the fact that magnetic clouds are only a subset of ICMEs, plus the spacecraft sampling of only those intercepting the spacecraft. Moreover, the total number of magnetic clouds in each year is small, thus statistical fluctuations are large. Finally, we only have a few incomplete solar cycles. We do not yet fully understand what separates magnetic clouds and non-cloud ICMEs. If clouds and non-cloud ICMEs were both generated as fluxropes near the solar surface and some of them are subsequently distorted in their propagation to 1AU (Odstrcil and Pizzo, 1999; Burlaga et al., 2002), the number of magnetic clouds (only) in each year and its solar cycle evolution does not represent the real picture. Rather the important observation here is the phase of the solar cycle when magnetic cloud polarity reverses.

Based on results presented in this paper together with the PVO results of Mulligan et al. (1998), the following statements can be made with reasonable confidence. SN magnetic clouds prevail over NS magnetic clouds in an odd solar cycle and the reverse is true for an even solar cycle. The prevailing polarity becomes less dominant towards the solar minimum, while the secondary polarity magnetic clouds start to increase in number, but the latter only become dominant after the later part of the declining phase. Therefore, the predominance of the magnetic cloud polarity reverses within the later part of the declining phase near the solar minimum, but does not coincide with either the solar minimum when the new polarity sunspots begin to emerge or the solar maximum when the large scale solar polar field reverses (see top panel in Fig. 2). Our results here have a more complex picture, while the PVO results showed a simpler trend. The total number of bipolar magnetic clouds and unipolar magnetic clouds shown in Fig. 3 are not well ordered by the solar cycle, unlike the findings of Mulligan et al. (1998) using PVO data at 0.7 AU during 1979–1988. Based on the solar cycle distribution of the total number of bipolar and unipolar magnetic clouds shown in Fig. 5 in Mulligan et al. (1998), they concluded the orientation of the fluxropes of the magnetic clouds is ordered by the solar large scale field. However, the results of our study do not fully support their conclusion. Perhaps both solar polar field cycle and the Hale active region polarity cycle may affect the magnetic cloud polarity. We suspect that because magnetic clouds may come from different source regions, subgroups of magnetic clouds may give different pictures of the solar cycle evolution, e.g., magnetic clouds related to filament or active region versus helmet streamer belt eruptions, but this will require a different study to relate each magnetic cloud to its source region. It is also interesting to note the following. Interplanetary shock statistics indicate that ICMEs are more frequent around solar maximum (Webb and Howard, 1994; Lindsay et al., 1995). In contrast, the total number of magnetic clouds does not show a simple solar cycle trend from the results of this study. How the ratio between magnetic clouds and non-cloud ejecta varies with the solar cycle and what causes it will be an interesting question and will be the topic for a future study.

4. Geoeffectiveness of the magnetic clouds

4.1. NS magnetic clouds versus SN magnetic clouds

For a statistical study of the geoeffectiveness of the NS and SN magnetic clouds and their surrounding solar wind disturbances, we combine the events found in both periods described in earlier sections. Magnetic clouds identified in IMP8 data from 1983 to 1992 are also included. As described earlier in Section 2, IMP8 has less than 50% coverage of the upstream solar wind. Only 6 NS magnetic clouds and 2 SN magnetic clouds are identified with confidence in IMP8 data. We have 25 NS magnetic clouds and 60 SN magnetic clouds total. Taking the D_{st} values from the Kyoto D_{st} index service (http://swdcdb.kugi.kyoto-u.ac.jp/dstdir/) as a measure of geomagnetic storms, the minimum D_{st} values related to NS magnetic clouds range from -20 to -250 nT, and to SN magnetic clouds range from -20 to -330 nT. The largest storms in our sample were apparently caused by SN magnetic clouds. In Fig. 4, we present the minimum D_{st} values of each storm grouped by year. The plus signs represent storms related to the NS magnetic clouds and diamond signs represent storms related to the SN magnetic clouds. The distributions of absolute values of the minimum D_{st} in Fig. 5 are generated with the bin size of 25 nT, where the full line represents storms related to NS magnetic clouds and dashed line represents storms related to SN magnetic clouds. Since the total number of samples is small for both groups,

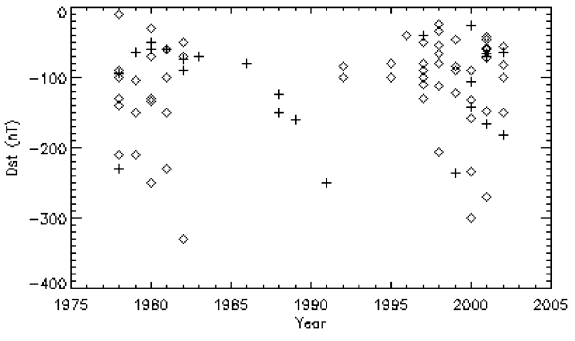

Fig. 4. The minimum D_{st} values grouped by year. The pluses represent geomagnetic storms caused by NS magnetic clouds and the diamonds represent geomagnetic storms caused by SN magnetic clouds.

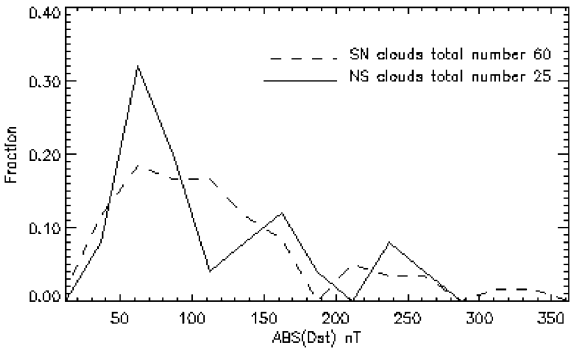

Fig. 5. Histogram showing the distribution of the absolute minimum D_{st} values associated with NS magnetic clouds (full line) and with SN magnetic clouds (dashed line).

the fluctuations are expected to be large and the exact shape of the distribution may not be significant. From these distributions, we do not find substantial difference in geo-effectiveness between the two types of magnetic clouds together with their associated surrounding solar wind disturbances.

In Table 1, we summarized the number of geomagnetic storms under three D_{st} ranges and the corresponding number of storms caused by magnetic cloud periods regardless of the magnetic cloud polarity. One can see that magnetic cloud periods are responsible for approximately one-third of the total geomagnetic storms, leaving two-thirds due to other disturbances including non-cloud ejecta and solar wind stream interactions. But most (over 70%) of the storms stronger than -200 nT were caused by the disturbances due to the magnetic clouds (Gosling et al., 1991; Richardson et al., 2001; Huttunen et al., 2002).

We summarized in Table 2 the number of storms in the three solar cycles, with cycle 23 only partial at this time. The number of storms in each solar cycle is comparable at all three D_{st} ranges. We have discussed earlier the observation that in solar cycle 21 and 23, the majority of magnetic clouds are SN polarized, and in solar cycle 22, the majority are NS polarized. This supports the argument that the two types of magnetic clouds should be almost equally geoeffective.

Among the 46 bipolar magnetic clouds during 1995–2002, 13 of them (28.3%) were compressed from behind by fast solar wind streams, which is below the ratio 40–45% given in Fenrich and Luhmann (1998). But among the 31 bipolar magnetic clouds during 1978–1982, only five of them (16%) were in this category. Out of all the compressed cases, only four are NS magnetic clouds. While we believe the Fenrich and Luhmann effect is true for individual cases, i.e., NS magnetic clouds might cause larger geomagnetic storms versus SN magnetic clouds under the circumstances that the magnetic clouds should be followed and compressed from the behind by fast solar wind streams, this data set cannot provide evidence for its significance statistically. More samples of NS magnetic clouds are needed. Though if we compare the number of storms in the three solar cycles in Table 2, no substantial difference is seen among all ranges of storms. Perhaps the effect is not statistically important.

We took a close look at the detailed cloud and solar wind structures when the six extremely intense storms ($-301 \geqslant D_{st} \leqslant -200$ nT) occurred during 1995–2002 period, and found two cases when SN clouds combined with sheath B_z south; two cases when SN clouds have large internal B_z south and high speed; one case when a NS cloud is compressed from behind by a fast solar wind stream; and one case with a N unipolar cloud when a very large B_z south in the sheath was responsible for the storm. During the 1978–1982 period, there were seven extremely intense storms ($-330 \geqslant D_{st} \leqslant -200$ nT) caused by our selected cloud disturbances. We found four cases when there are large internal B_z south in the cloud and high speed; one case when there is a very large internal B_z south and medium speed; two cases when the SN clouds combined with B_z south in sheath, and high speed. Related studies of intense storm conditions in interplanetary space can be found in, e.g., Gonzalez et al. (2002).

4.2. Significance of magnetic cloud portion

A geomagnetic storm is usually the result of a disturbed solar wind period with an out of ecliptic plane magnetic field component, especially southward B_z. In the case of magnetic clouds, as described earlier, the disturbed period may include a shock, the sheath, and the magnetic cloud, also

Table 1

Year	D_{st} range (nT)	(1) Number of geomagnetic storms	(2) Number of storms by clouds	Ratio (%) (2)/(1)
1978–1982	$\leqslant -50$	153	37	24.2
(in cycle 21)	$\leqslant -100$	58	18	31.0
	$\leqslant -200$	10	7	70
1995–2002	$\leqslant -50$	182	59	32.4
(mostly in	$\leqslant -100$	63	29	46.0
cycle 23)	$\leqslant -200$	8	6	75

Table 2

Solar Cycle	D_{st} range (nT)	Number of geomagnetic storms
Cycle 21	$\leqslant -50$	239
(1976–1985)	$\leqslant -100$	77
	$\leqslant -200$	10
Cycle 22	$\leqslant -50$	256
(1986–1995)	$\leqslant -100$	84
	$\leqslant -200$	9
Cycle 23[a]	$\leqslant -50$	171
(1996–July/2003)	$\leqslant -100$	61
	$\leqslant -200$	8

[a]Cycle 23 is incomplete at the time of this work.

sometimes with a fast solar wind stream pushing the rear of the magnetic cloud. We examine here how significantly the magnetic cloud portion of the disturbed period contributes to the geoeffectiveness. For this purpose, the Burton empirical D_{st} formula (Burton et al., 1975) is used with the required solar wind and IMF parameters (proton density, solar wind bulk speed, and B_z) taken only within the magnetic cloud portion of the disturbed periods. The D_{st} values calculated in this way approximate the storm index that would be produced if the magnetic cloud existed in isolation in the solar wind (no ambient solar wind structure or sheath). The formula used is

$$\frac{d(D^*_{st})}{dt} = F(E) - aD^*_{st}, \tag{1}$$

where

$$D^*_{st} = D_{st} - b\sqrt{P_{dyn}} + c \tag{2}$$

and

$$F(E) = 0, \quad E_y < 0.5 \text{ mV/m} \tag{3}$$

$$F(E) = d(E_y - 0.5), \quad E_y > 0.5 \text{ mV/m} \tag{4}$$

with

$a = 3.6 \times 10^{-5}$ s^{-1}

$b = 0.20$ nT$/\sqrt{\text{eV/cm}^3}$

$c = 20$ nT

$d = -1.5 \times 10^{-3}$ nT/(smV/m).

In the above equations, D^*_{st} is the change to D_{st} from only the injected ring current. The constant b is a measure of the D_{st} response to solar wind dynamic pressure (P_{dyn}), while c is a measure of the quiet time ring current. $F(E)$ is the ring current injection rate and only depends upon the dawn to dusk solar wind electric field, E_y, which is given by $-(V \times B)y$, V being the solar wind velocity and B the IMF.

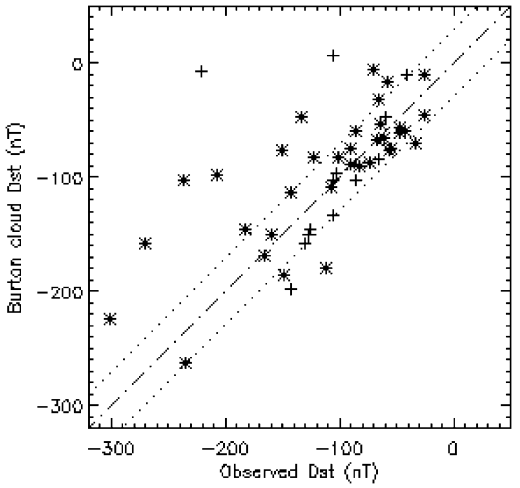

Fig. 6. Scatter plot of the minimum observed D_{st} and estimated minimum cloud D_{st} using Burton formula, where star signs represent 35 bipolar magnetic clouds and plus signs for 13 unipolar magnetic clouds.

The constant d is a measure of the response of the injection rate to E_y that is assumed to be linear, and the parameter a is a measure of a ring current decay, the value of which corresponds to an e-folding time of 7.7 h in our study.

We use data from the ACE period when both solar wind and IMF data have the best quality to perform this calculation. In Fig. 6, a scatter plot of the minimum D_{st} values from the Kyoto observations versus the estimations of cloud-only-storm minimum D_{st} values (Burton cloud D_{st}) for the same group of events using the above formula and cloud data is shown.

The star signs represent the 35 bipolar magnetic clouds and the plus signs the 13 unipolar magnetic clouds. Approximately 60% of the cases are near the diagonal line (slope = 1) within ±30 nT, which means these clouds make the sole or major contributions to the storm. About 30% of the cases are in the upper left, which tells us that the observed storms are not solely by the clouds, but other contributions were significant. The difference between the observed minimum D_{st} and the minimum estimated cloud D_{st} can be as large as −200 nT. We examined details of 13 cases when the differences are greater than −30 nT, and found the following. There are 10 cases when the sheath has south B_z that significantly contributed to the storms, one case when there was a fast solar wind stream compressing the CME from behind and the compressed density portion was not included in our cloud boundary, one case when there was another faster CME compressing the cloud from behind and two cases when the reasons are unknown. Included in the 13 cases, there are 2 N unipolar clouds, when the storms should be caused solely by the sheath, which are the two plus signs at the top of the plot with estimated minimum

cloud D_{st} around zero. Also two cases are somewhat further below the diagonal line, no cases are to the far lower right. With one of the two cases, the reason for the fact that the observed storm is weaker than estimated by only cloud portion of the disturbance is unknown. With the second case, there is a compression to the geomagnetosphere and the D_{st} value increased to a positive value (~ 40 nT) prior to the storm. Of course, in interpreting these results, one must keep in mind the approximate nature of the Burton empirical formula. However, it has been shown to perform remarkably well in spite of its simplicity (e.g., Lindsay et al., 1999).

4.3. Discussions on geoeffectiveness

In Fig. 4, it is seen that in cycle 21, all the geomagnetic storms with the minimum D_{st} less than -100 were caused by SN magnetic clouds. In cycle 23, on the other hand, the ratio between the number of strong magnetic storms caused by SN magnetic clouds and that by NS magnetic clouds is moderate as 3:1. In cycle 22, we do not have the complete picture, but the four strong geomagnetic storms with the minimum D_{st} less than -100 are all caused by NS magnetic storms. These trends are interesting for space weather predictions, but based on the results we have now, it is not conclusive. From the distribution presented in Fig. 5 and the statistics of the number of storms in Tables 1 and 2, the overall geoeffectiveness of the two types (NS and SN) of magnetic clouds are not significantly different.

The comparison between the observed minimum D_{st} values and estimated minimum D_{st} values using the Burton empirical formula showed that approximately half of the time the cloud portion of the disturbance provides the sole or major contribution to the resulting geomagnetic storm, and often (about 30% of the cases) the sheath portion of the magnetic cloud period provides significant contribution to the storm. Other contributions are much less in this study. The sheath portion of the magnetic cloud period often carries south B_z component as the magnetic field contained usually oscillates with a large magnitude. It is rare for a sheath portion to have a long lasting steady B_z south, but a short large B_z south combined with large dynamic pressure, which is almost always the case in the sheath, often contribute significantly to the storm, especially when the magnetic B_z field in the magnetic cloud behind the sheath is south first (SN or S magnetic clouds). This combination is a major one during the ISEE3 and WIND-ACE periods.

We also found that magnetic cloud periods are responsible in causing only one-third of the total number of geomagnetic storms among other disturbances including non-cloud ejecta, solar wind stream interactions, etc. However, it is evident that magnetic cloud periods (including the sheath, the cloud, etc.) are responsible for the most intense geomagnetic storms (Gosling et al., 1991; Richardson et al., 2001; Huttunen et al., 2002).

5. Conclusions

This study has focused on the solar cycle trends in magnetic cloud occurrence and polarities and their possible influence on geomagnetic storm strength. Our results on the solar cycle trends in magnetic cloud polarities, involving almost three solar cycles (the longest duration magnetic cloud polarity study to date), suggest that their polarity change does not occur around solar maximum together with the solar polar field polarity reversal. Neither does it occur at the solar minimum with the appearance of new cycle active regions. Rather, it occurs during the later declining phase of the solar cycle, a finding that must be explained by further effort including, as suggested earlier, studies that discriminate magnetic clouds according to different source regions, and models of CMEs and ICMEs. While the previously suggested simpler pictures of filament related field control of magnetic cloud polarity (Webb, 1988; Bothmer and Schwenn, 1998; Martin and McAllister, 1997) or large-scale solar field control of magnetic cloud polarity (Mulligan et al., 1998) may describe some observations, we find that the relation between magnetic clouds in the solar wind and the near solar surface source region fields is more complicated (also see Leamon et al., 2002). Both large-scale magnetic cycle and Hale solar activity cycle may contribute to the long-term variation of some CME characteristics. This is not inconsistent with findings that some CMEs are clearly related to solar flares and active regions, disappearing filaments (Webb, 1988; Martin and McAllister, 1997; Leamon et al., 2002), others are not apparently related to any small-scale solar activities, but possibly involving large scale solar magnetic fields, such as coronal helmet streamer fields (Gosling, 1990; Crooker et al., 1993; Luhmann et al., 1998; Li et al., 2001). Violent changes of the coronal helmet streamer during CMEs are often observed in white light coronagraph images (Subramanian et al., 1999). Our study of geoeffectiveness of magnetic clouds indicates that regardless of polarity, they are important intense storm producers. The need to understand the subset of ICMEs called magnetic clouds is clearly a high priority in space weather research. Ongoing efforts to more realistically model CMEs, together with closer examinations of source region and ICME pairs are necessary for a further understanding.

Acknowledgements

This work is supported in part by CISM, which is funded by the STC Program of the NSF as agreement ATM-0120950. The authors are also partly supported by the Solar MURI project. The authors would like to thank Dr. C. T. Russell and assistant for their kindly providing most of the data sets used in this study. We also thank the Principal Investigators of the in-situ experiments on ACE, WIND, ISEE3 and IMP8 for making their data publicly available, and the NSSDC at Goddard Space Flight Center for providing it for retrospective study.

References

Bothmer, V., Rust, D.M., 1997. The Field Configuration of Magnetic Clouds and the Solar Cycle, Coronal Mass Ejections. AGU Geophysical Monograph, Vol. 99. AGU, Washington, DC, pp. 139–146.

Bothmer, V., Schwenn, R., 1998. The structure and origin of magnetic clouds in the solar wind. Annales Geophysicae 16, 1–24.

Burlaga, L.F., 1991. Magnetic clouds. In: Schwenn, R., Marsch, E. (Eds.), Physics of the Inner Heliosphere, Vol. II. Springer, Berlin, Heidelberg, pp. 1–22.

Burlaga, L.F., Plunkett, S.P., St Cyr, O., 2002. Successive CMEs and complex ejecta. Journal of Geophysical Research 107 (A10), 1266–1277.

Burton, R.K., McPherron, R.L., Russell, C.T., 1975. An empirical relationship between interplanetary conditions and Dst. Journal of Geophysical Research 80, 4204–4214.

Crooker, N.U., Siscoe, G.L., Shodhan, S., Webb, D.F., Gosling, J.T., Smith, E.J., 1993. Multiple heliospheric current sheets and coronal streamer belt dynamics. Journal of Geophysical Research 98 (A6), 9371–9381.

Fenrich, R.R., Luhmann, J.G., 1998. Geomagentic response to magnetic clouds of different polarity. Geophysical Research Letters 25, 2999–3002.

Garrard, T.L., Davis, A.J., Hammond, J.S., Sears, S.R., 1998. The ACE science center. Space Science Reviews 86 (1–4), 649–663.

Gonzalez, W.D., Tsurutani, B.T., Lepping, R.P., Schhwenn, R., 2002. Interplanetary phenomena associated with very intense geomagnetic storms. Journal of Atmospheric and Solar-Terrestrial Physics 64, 173–181.

Gosling, J.T., 1990. Coronal mass ejections and magnetic flux ropes. In: Russell, C.T., Priest, E.R., Lee, L.C. (Eds.), Interplanetary Space. AGU Geophysical Monograph, Vol. 58. AGU, Washington, DC, pp. 343–364.

Gosling, J.T., McComas, D.J., Phillips, J.L., Bame, S.J., 1991. Geomagnetic activity associated with earth passage of interplanetary shock disturbances and coronal mass ejections. Journal of Geophysical Research 96, 7831–7839.

Huttunen, K.E.J., Koskinen, H.E.J., Schwenn, R., 2002. Variability of Magnetospheric storms driven by different solar wind perturbations. Journal of Geophysical Research (Space Physics) 107(A7), SMP 20–1.

Leamon, R.J., Canfield, R.C., Pevtsov, A.A., 2002. Properties of magnetic clouds and geomagnetic storms associated with eruption of coronal sigmoids. Journal of Geophysical Research 107 (A9), 1234–1242. doi:10.1029/2001JA000313.

Li, Y., Luhmann, J.G., Mulligan, T., Hoeksema, J.T., Arge, N., 2001. Earthward directed CMEs seen in large-scale coronal magnetic field changes in SOHO LASCO coronagraph and solar wind. Journal of Geophysical Research 106, 25,103–25,120.

Lindsay, G.M., Luhmann, J.G., Russell, C.T., Gazis, P., 1995. Solar cycle variation of interplanetary shocks, coronal mass ejections, and stream interactions observed at 0.7 AU. Advances in Space Research 16 (9), 353–354.

Lindsay, G.M., Russell, C.T., Luhmann, J.G., 1999. Predictability of D_{st} index based upon solar wind conditions monitored inside 1 AU. Journal of Geophysical Research 104, 10335–10344.

Luhmann, J.G., Gosling, J.T., Hoeksema, J.T., Zhao, X.P., 1998. The relationship between large scale solar magnetic field evolution and coronal mass ejections. Journal of Geophysical Research 103, 6585–6594.

Martin, S.F., McAllister, A.H., 1997. Predicting the sign of helicity in erupting filaments and coronal mass ejections. In: Crooker, N.U., Joselyn, J.A., Feynman, J. (Eds.), Coronal Mass Ejections, Geophysical Monograph, Vol. 99. AGU, Washington, DC, pp. 127–138.

Mulligan, T., Russell, C.T., 2001. Multispacecraft modeling of the flux rope structure of interplanetary coronal mass ejections: cylindrically symmetric versus nonsymmetric topologies. Journal of Geophysical Research 106, 10581–10596.

Mulligan, T., Russell, C.T., Luhmann, J.G., 1998. Solar cycle evolution of the structure of magnetic clouds in the inner heliosphere. Geophysical Research Letters 25, 2959–2962.

Odstrcil, D., Pizzo, V.J., 1999. Distortion of the interplanetary magnetic field by three-dimensional propagation of coronal mass ejections in a structured solar wind. Journal of Geophysical Research 104, 28225–28239.

Paularena, K.I., King, J.H., 1999. NASA's IMP 8 spacecraft. In: Sibeck, D.G., Kudela, K. (Eds.), Interball in ISTP Program, NATO Science Series, Series C. Dordrecht, The Netherlands. Vol. 537, pp. 145–154.

Richardson, I.G., Cliver, E.W., Cane, H.V., 2001. Sources of geomagnetic storms for solar minimum and maximum conditions during 1972–2000. Geophysical Research Letters 28, 2569–2572.

von Rosenvinge, T.T., 1982. Data from ISEE-3 for the IMS period. In: Russell, C.T., Southwood, D.J. (Eds.), The IMS Source Book: Guide to the International Magnetospheric Study data analysis (A83-16276 04-46). AGU, Washington, DC, pp. 1–9.

Russell, C.T. (Ed.), 1995. The Global Geospace Mission. Space Science Reviews 71, 1–4.

Subramanian, P., Dere, K.P., Rich, N.B., Howard, R.A., 1999. The relationship of coronal mass ejections to streamers. Journal of Geophysical Research 104, 22321–22330.

Webb, D.F., 1988. Erupting prominence and the geometry of coronal mass ejections. Journal of Geophysical Research 93, 1749–1758.

Webb, D.F., Howard, R.A., 1994. The solar cycle variation of coronal mass ejections and the solar wind mass flux. Journal of Geophysical Research 99 (A3), 4201–4220.

Zhang, G., Burlaga, L.F., 1988. Magnetic clouds, geomagnetic disturbances and cosmic ray decreases. Journal of Geophysical Research 93, 2511–2518.